

PUBLISHED VERSION

Lu Peng, Nicolas Riesen, Jiawen Li, Mengke Han, Linh Viet Nguyen, Heike Ebendorff-Heidepriem, and Stephen C. Warren-Smith

Whispering gallery mode excitation using exposed-core fiber

Optics Express, 2021; 29(15):23549-23557

DOI: <http://dx.doi.org/10.1364/OE.431544>

© 2021 Optical Society of America under the terms of the OSA Open Access Publishing Agreement. Authors and readers may use, reuse, and build upon the article, or use it for text or data mining without asking prior permission from the publisher or the Author(s), as long as the purpose is non-commercial and appropriate attribution is maintained.

PERMISSIONS

https://opg.optica.org/submit/review/copyright_permissions.cfm#posting

Author and End-User Reuse Policy

Our policies afford authors, their employers, and third parties the right to reuse the author's Accepted Manuscript (AM) or the final publisher Version of Record (VoR) of the article as outlined below:

Reuse purpose	Article version that can be used under:		
	Copyright Transfer	Open Access Publishing Agreement	CC BY License
Posting by authors on an open institutional repository or funder repository	AM after 12 month embargo	VoR	VoR

Attribution

Open access articles

If an author or third party chooses to post an open access article published under our OAPA on his or her own website, in a repository, on the arXiv site, or anywhere else, the following message should be displayed at some prominent place near the article and include a working hyperlink to the online abstract in the journal:

© XXXX [year] Optica Publishing Group. Users may use, reuse, and build upon the article, or use the article for text or data mining, so long as such uses are for non-commercial purposes and appropriate attribution is maintained. All other rights are reserved.





When adapting or otherwise creating a derivative version of an article published under our OAPA, users must maintain attribution to the author(s) and the published article's title, journal citation, and DOI. Users should also indicate if changes were made and avoid any implication that the author or Optica Publishing Group endorses the use.

27 March 2023

<https://hdl.handle.net/2440/131683>



Whispering gallery mode excitation using exposed-core fiber

LU PENG,^{1,2,3,*} NICOLAS RIESEN,^{2,4}  JIAWEN LI,^{2,3,5}  MENGKE HAN,^{1,2,3} LINH VIET NGUYEN,^{1,2} HEIKE EBENDORFF-HEIDEPRIEM,^{1,2,3}  AND STEPHEN C. WARREN-SMITH^{1,2,3,4} 

¹*School of Physical Sciences, The University of Adelaide, Adelaide, SA 5005, Australia*

²*Institute for Photonics and Advanced Sensing, The University of Adelaide, Adelaide, SA 5005, Australia*

³*Australian Research Council Centre of Excellence for Nanoscale Biophotonics, The University of Adelaide, Adelaide, SA 5005, Australia*

⁴*Future Industries Institute, University of South Australia, Mawson Lakes, SA 5095, Australia*

⁵*Adelaide Medical School, The University of Adelaide, Adelaide, SA 5005, Australia*

*lu.peng@adelaide.edu.au

Abstract: Whispering gallery modes (WGMs) in micro-resonators are of interest due to their high Q-factors. Ultra-thin fiber tapers are widely deployed to couple light into micro-resonators but achieving stable and practical coupling for out-of-lab use remains challenging. Here, a new WGM coupling scheme using an exposed-core silica fiber (ECF) is proposed, which overcomes the challenge of using fragile fiber tapers. Microspheres are deposited onto the exposed channel for excitation via the evanescent field of the fiber's guided modes. The outer jacket of the ECF partially encapsulates the microspheres, protecting them from external physical disturbance. By varying the mode launching conditions in this few-mode ECF, in combination with a Fano resonance effect, we demonstrate a high degree of tunability in the reflection spectrum. Furthermore, we show multi-particle WGM excitation, which could be controlled to occur either simultaneously or separately through controlling the ECF mode launching conditions. This work can bring value towards applications such as optical switches and modulators, multiplexed/distributed biosensing, and multi-point lasing, integrated in a single optical fiber device that avoids fiber post-processing.

© 2021 Optical Society of America under the terms of the [OSA Open Access Publishing Agreement](#)

1. Introduction

Electromagnetic waves can circulate within micro-cavities based on total internal reflection, a phenomenon known as whispering gallery mode (WGM) resonance. This leads to strong resonances useful for many applications including biochemical sensing, lasing, and nonlinear/quantum optical devices [1–3]. Earlier reports have utilized prism or fiber taper coupling for the excitation of WGMs with more recent demonstrations using microstructured optical fibers [4–12]. While fiber tapers have been used widely to excite micro-resonators with high Q-factors up to 10^8 [2,3], handling the fragile micro-scaled tapered region and the requirement of a supporting platform to position the fiber and resonator remains challenging (e.g., for in-vivo applications). Integrated fiber couplers have been reported by melting a sphere at the tip of the optical fiber [13,14] or etching/melting the optical fiber to expose the core while retaining the outer fiber structure to hold the resonator [15–18]. Although they are portable and potentially suitable for out-of-lab use, the melting/etching procedures are time-consuming, produce fragile structures, and lack high repeatability.

An alternative approach is the use of suspended core microstructured fibers (SCFs), which have the advantage of using the built-in air channels to immobilize resonators [4,6,8]. In these studies, either capillary action was used to encapsulate the particle inside one of the SCF air channels, or the particles were positioned at the SCF end-face. In either case there is limited

ability to manipulate the position of the particles and distributed multi-resonator placement is difficult. Similar to SCFs, exposed core microstructured optical fibers (ECFs) provide an accessible evanescent field along the entire fiber length but with an exposed channel to allow direct access to the core from the surrounding environment at any location along the fiber [19]. This is similar to a D-shaped optical fiber, but for comparable core diameters the evanescent field of the ECF is several times higher (depending on the specific mode) [20]. The ECF also avoids the preform or fiber polishing/micromachining required to fabricate D-shaped fibers [21–23], which can be difficult to avoid cracking the optical core of the preform or to control the precise depth in the case of polishing the fiber. Our work has recently demonstrated that the ECF is a good candidate to be deployed for distributed sensing, including the detection of micro-scaled particles [24,25].

In this paper, we present a new scheme for exciting micro-resonator WGMs. Having standard fiber dimensions (160 μm) and the ability to be drawn with kilometer lengths, the ECF overcomes the fragility of using ultra-thin fiber tapers and avoids fiber post-processing (i.e., tapering, etching, melting, and polishing). Furthermore, the microspheres could be positioned on the exposed surface in a controllable way due to the direct access provided by the open side channel, allowing the WGMs to be excited via the evanescent field of the guided modes of the ECF. We show that by controlling the mode launching into the few-mode ECF, the spectrum can be switched between transmission and reflection of the resonant wavelengths through a Fano resonance interaction. Furthermore, the scheme is naturally amenable to multi-resonator coupling, which we demonstrate by exciting WGMs in two microspheres with different sizes on the exposed channel either separately or simultaneously. Our scheme holds potential as a tunable reflector or filter for integrated photonic processing or as a platform for multi-point sensing/lasing and slow light [26].

2. Experimental setup

The WGM fiber coupler is shown in Fig. 1(a), where light from a swept source interrogator (National Instruments, PXIe-4844, 1510 - 1590 nm, 4 pm resolution, sampling rate 10 Hz) is injected into the ECF core. The ECF cross-section is shown in Fig. 1(b), with a core diameter of 5.4 μm , which was fabricated in-house as previously reported in [27]. Several simulated (COMSOL 5.3) ECF modes are presented in the bottom of Fig. 1(a), where the fundamental mode is labeled as 'FM' and other higher-order modes are shown as 'HOM' followed by sequential integers (1-7), with corresponding effective mode index listed below each image at a wavelength of 1550 nm. The WGM excitation of a polystyrene microsphere via the ECF evanescent field is illustrated in Fig. 1(c). The reflected light [indicated by the red arrow in Fig. 1(c)] from the microspheres is then recoupled into the ECF's guided modes and detected by the interrogator. Meanwhile, the near-field ECF output from the far end of the fiber is monitored using an InGaAs camera. Note that the reflection configuration used here is to reduce the background signal from the light source to allow WGM signals to be observed, as the coupling efficiency in this relatively large core ECF is low due to the limited evanescent field.

An image of the ECF with microsphere placed onto the core is presented in Fig. 1(d), where a 20 μm polystyrene sphere (Thermo Fisher: Duke Standards 2020A, refractive index: 1.59 at 589 nm) was located 29 μm away from the ECF input, and the magnified image is shown in Fig. 1(e). To deposit the particles, a droplet (1 μL) of polystyrene sphere solution (diluted in milli-Q water: 0.04 g/cm^3) was placed inside the exposed channel and the microspheres were deposited inside the channel while the water was evaporated after tens of seconds. Then, microspheres were positioned inside the exposed channel using a tapered micro-scaled glass tube, which was controlled by a three-axis translation stage under an optical microscope. The polystyrene spheres adhere to the ECF (silica) surface through physisorption unless there is a

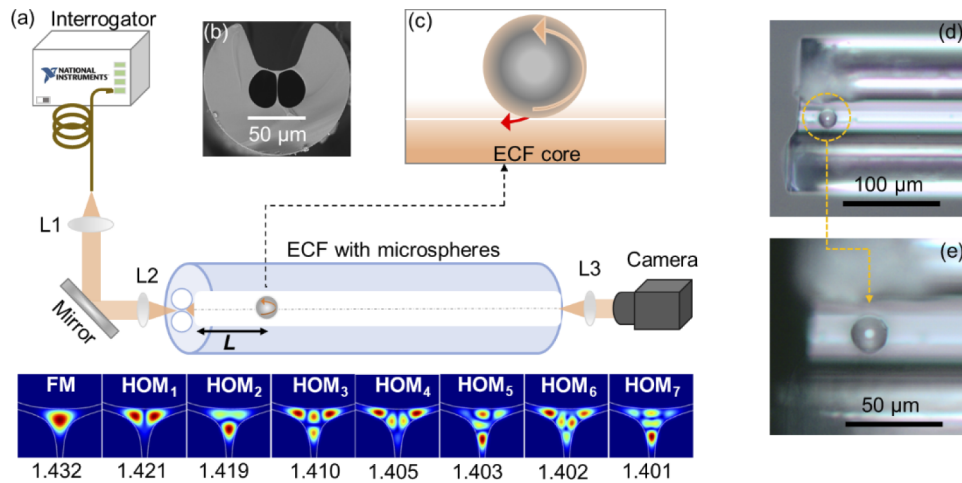


Fig. 1. Experimental set-up and the fiber sample (length: 220 mm) used for the experiments. (a) Schematic diagram based on reflection detection, while simulated modes are shown in the bottom. (b) Scanning electron microscope image of the ECF cross-section. (c) Illustration of WGM excitation based on the evanescent field. (d) Microscope image: a polystyrene sphere located on the input side of the ECF exposed channel, while the magnified image is in (e).

destructive mechanical force from the outside environment. The ECF input end was angle-cleaved (6.2°) to avoid strong reflections.

3. Results

3.1. Fabry-Perot interference

An example reflection spectrum is shown in Fig. 2(a), which results from the mode launching shown by the output near-field image in the inset. The spectrum exhibits weak Fabry-Perot (FP) interference with a free spectral range (FSR) of 35 nm. This corresponds to the physical distance between the ECF input and the located sphere and is apparent in the fast Fourier transform (FFT) in Fig. 2(b).

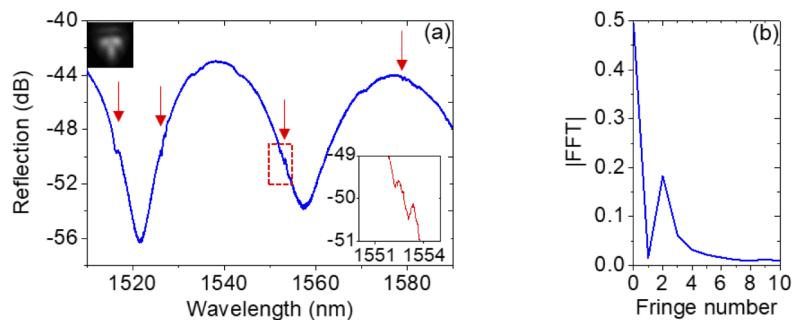


Fig. 2. (a) Large interference fringes from the FP cavity formed between the ECF input and the microsphere). Red arrows indicate the occurrence of WGMs. Inset shows a magnified view of the spectrum in the red dashed box. The near-field output image is at top left. (b) The absolute FFT calculated from the spectrum of (a).

The FSR in the wavelength domain is determined by the expression:

$$FSR_{\Delta\lambda} = \lambda^2 / 2n_g L. \quad (1)$$

where L is the physical length of the FP cavity [marked in Fig. 1(a)], n_g is the group index of the propagating optical fiber mode within the cavity, and λ is the center wavelength (1550 nm) of the light source.

The calculated FSR of the FP (input-sphere) cavity is 29 nm using a calculated group index of 1.44 [HOM₂ shown in the bottom of Fig. 1(a)], which is in reasonable agreement with the measured result. The error is primarily due to both the angle of the cleave (it is not easy to define the exact edge of the ECF core position under the optical microscope to determine the exact distance), error in the group index calculated in the numerical model, and modal dispersion due to a superposition of the excited modes. Several small features are observed in the reflection spectrum in Fig. 2(a) shown by the arrows (the red dashed box region is magnified in the inset), which are indicative of the WGM resonances and we now investigate in detail. In particular, we now see how the presence of the background FP interference and the WGM excitation leads to the potential of Fano resonance interactions resulting from the interference between a continuum and a discrete state [28,29].

3.2. Fano resonance

Fano resonances can occur through interaction between micro-resonators and external cavities such as FP interferometers, which not only allows for higher sensitivity due to the narrower linewidth but can also be used for photonic switches due to sharp tuning between reflection and transmission features [28,30–32]. In our work, the launching conditions were manually adjusted by changing the transverse dimensions (i.e., x and y axes) of a three-axis optical stage used to free-space launch the laser beam into the ECF. The degree of the reflection from the angle-cleaved ECF returned to the interrogator was then used to tune the Fano resonance, while the WGM excitation was simultaneously adjusted due to the variation of the launched modes. This is demonstrated in Figs. 3(a-c), where three different reflection spectra are shown using the same sample under different launching conditions. In this case the launching was adjusted to yield strong WGM resonance features. The mode images (insets in Fig. 3) show that the launched modes were not primarily the fundamental (Gaussian) mode, but rather that higher-order modes of the ECF were phase-matched to the 20 μm polystyrene sphere's WGMs. Extracted signal features from 1575 to 1585 nm are presented in Fig. 3(a1, b1, c1) to show the peaks more clearly, while the corresponding FFTs are presented in Fig. 3(a2, b2, c2). The resonance condition for the transverse electric (TE) and transverse magnetic (TM) WGMs are given by [33]:

$$n_p^p \frac{\psi_l'(n_p k_0 \rho)}{\psi_l(n_p k_0 \rho)} = n_s^p \frac{\chi_l'(n_s k_0 \rho)}{\chi_l(n_s k_0 \rho)}. \quad (2)$$

where n_p is the index of the microsphere, n_s is the surrounding index, l is the azimuthal mode number, p is the polarization coefficient, k_0 is the resonance wavenumber, and ψ_l and χ_l are associated with spherical Ricatti-Bessel and Ricatti-Neumann functions. A summary of the theoretical TE and TM resonant wavelengths based on Eq. (2) are shown in Table 1 as a function of azimuthal mode number (radial mode number: $q = 1$), based on a polystyrene sphere (diameter of 20 μm, refractive index of 1.55) in the wavelength range of interest. The resonant peaks and troughs of the experimentally measured spectra ('A' and 'B' in Fig. 3) are also listed in the table for comparison. The azimuthal mode order alignment of 'A' and 'B' is based on the difference of resonant wavelength compared to the theoretical values under the same azimuthal mode order. In Table 1, the difference between each pair of experimentally measured adjacent peaks or troughs in series A (or B) is 25 to 27 nm, which matches well with the theoretical difference between

each adjacent TE (or TM) resonant wavelength. Therefore, the observed peaks and troughs in the reflection spectra from Fig. 3 are concluded to have occurred from WGM resonances.

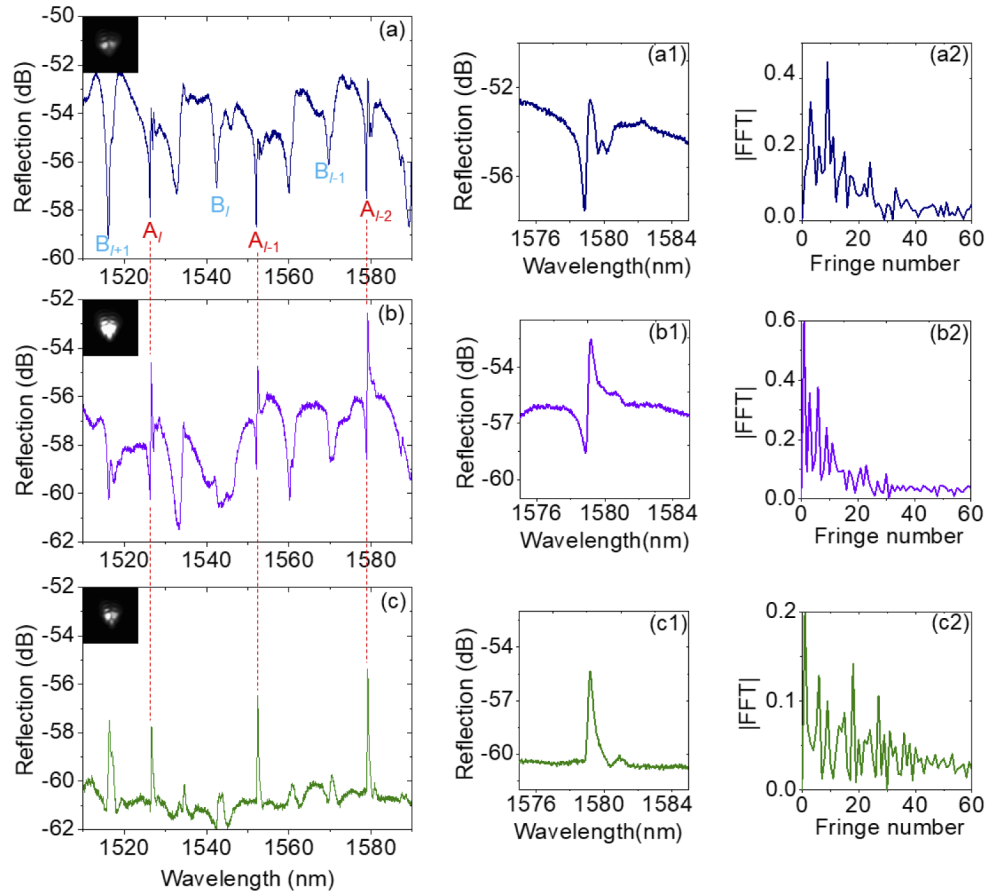


Fig. 3. Reflection spectra of observed WGMs under different launching conditions in (a), (b), and (c) with relevant near-field images captured from the far end of the ECF shown in the insets. Magnified reflection spectra are shown in (a1), (b1) and (c1). The corresponding FFTs are displayed in (a2), (b2) and (c2) with the same color, respectively.

Table 1. Simulated resonant wavelength of (20 μm sphere) WGMs.

Mode	$l+1$	l	$l-1$	$l-2$
TE	1515 nm	1539 nm	1563 nm	1589 nm
TM	N.A.	1522 nm	1546 nm	1571 nm
A	N.A.	1526 nm	1552 nm	1579 nm
B	1516 nm	1542 nm	1569 nm	N.A.

In theory, TE modes have longer resonant wavelengths compared to TM modes under the same azimuthal order according to Table 1. Therefore, the observed dips at positions ‘A’ in Fig. 3(a) are fundamental TM resonant modes ($q=1$), while ‘B’ series are fundamental TE resonant modes, and the remaining peaks and troughs are higher order radial modes ($q>1$) [7,15,17]. We have not

listed the exact value of l , which is estimated to be 57 ± 2 , as it is difficult to precisely assign due to errors in the size and refractive index of the polystyrene spheres in the simulation.

In addition, the FP cavity plays a significant role during the tuning of the spectrum under various launching conditions. This can be seen by the change in resonant peak properties under different mode launching conditions at positions 'A' indicated by the red dashed lines in Figs. 3(a-c). When the maximum of the FP interference varies around the sphere resonance wavelengths, it leads to Fano asymmetric features as shown in Fig. 3(a1) and (b1). Unlike Fig. 3(a1) and (b1), the reflection peaks in Fig. 3(c1) are purely from WGM resonances. This can be explained by the lower background (< -60 dB) as the reflection from the fiber input is not collected by the interrogator due to the cleaved angle under the specific launch conditions of the incident light. On the other hand, the spacing of the sharp peaks is 25 to 27 nm in Fig. 3(c), which is impossible to match with the three maxima of FP fringes (FSR=35 nm) to contribute three total reflections (with symmetric Lorentzian shapes) [32]. That is, at least one of the three resonant wavelengths [$A_{l-2}/A_{l-1}/A_l$ in Fig. 3(c)] would show an obvious Fano asymmetry if the FP interference was involved.

3.3. Coupling to multiple particles

To demonstrate multi-particle WGM excitation, a new fiber sample was prepared, initially by having a single 12 μm polystyrene sphere as shown in Fig. 4(a). Two reflection spectra were obtained as shown in Fig. 4(a1) with related (color matched) mode images at top. Two obvious peaks at 1515 and 1561 nm are from the fundamental TE mode with a wavelength spacing of 46 nm, which is well matched with theory, while small peaks at 1531 and 1577 nm are from the fundamental TM mode. We measured a Q-factor of 2.2×10^4 as shown in the magnified inset of Fig. 4(a1), which is comparable to other reported Q-factors using polystyrene spheres [5,6,8].

A second sphere with a diameter of 26 μm was then added to the same fiber as in-line as possible with the 1st sphere, with a center-to-center separation of 28 μm between the two spheres. The measured reflection spectra from the sample with two spheres are shown in Fig. 4(b1, b2). The two peaks shown at 1516 and 1562 nm in Fig. 4(b1) match with the spectra from the smaller original sphere in Fig. 4(a1), while the broader peak at 1522 nm is from the larger added sphere. In comparison, the peaks shown in the black spectrum in Fig. 4(b2) are dominantly from the 2nd larger sphere while those in the orange spectrum are dominantly from the 1st smaller sphere due to a slight difference in the ECF launching conditions. The WGM resonance from the second, larger, microsphere was relatively weaker compared to the first, smaller, microsphere, which is counter-intuitive given smaller microspheres generally have greater geometric loss leading to lower Q-factor. We attribute this to the fabrication variability of the microspheres (i.e., sphericity) for the particular excitation plane used in our experiments. Regardless, our results in Fig. 4 demonstrate that ECF mode launching can be controlled to excite WGMs in the two microspheres either separately or simultaneously.

Coupling between the two spheres is unlikely to have occurred in our case due to their large separation, but it could be considered in future work to investigate the evanescent coupling between several closely placed spheres/resonators (e.g., slow light) [26,34]. In future, it would also be possible to redesign the ECF geometry in order to hold and excite particles with a larger size (e.g., 50–200 μm silica spheres) to achieve even higher Q-factors [11]. Note that there is a trade-off between better Q-factor and higher sensitivity (wavelength shift) for sensing applications, where large spheres would contribute a higher Q-factor but relatively smaller wavelength shift during biosensing measurements [1]. Our current scenario with using small resonators would be particularly favorable for biosensing applications. Therefore, there is a range of flexibility for using the ECFs to couple into different spheres (size and material), to adjust either better Q-factor or sensitivity for serving specific purposes.

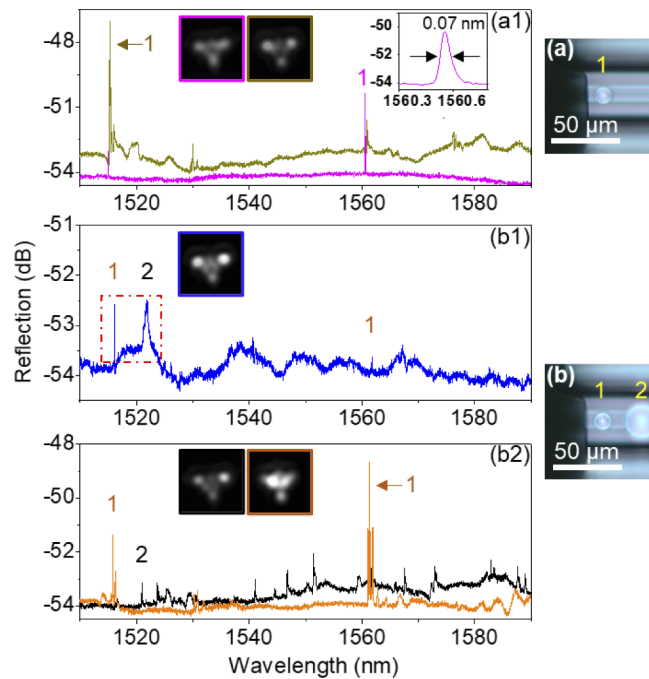


Fig. 4. Multi-particle WGM excitation. (a) ECF sample (length: 210 mm) with a single small polystyrene sphere. (a1) Two measured reflection spectra from the sample with a single sphere under different mode launching conditions (insets show corresponding near-field output). Inset: a magnified peak at 1561 nm to show the achievable high Q-factor using a small microsphere. (b) A large sphere is added on the ECF without changing the 1st small sphere. (b1) Reflection spectrum from the sample with two microspheres, showing the simultaneous excitation of WGMs from both microspheres. (b2) Reflection spectrum from the sample with two microspheres, showing either predominantly exciting WGMs in the small microsphere (orange) or the larger microsphere (black).

4. Conclusions and outlook

We have proposed and demonstrated an evanescent field WGM excitation scheme using an ECF. In addition to being a robust platform for WGM excitation, we show that by controlling the mode launching conditions of this few-moded fiber, combined with a Fano resonance effect, we have a high degree of flexibility in tuning the resulting reflection spectrum. In particular, multi-particle WGM excitation has been achieved in a single fiber either simultaneously or separately via adjustment of the mode launching conditions. We now outline several practical and optical refinements to our approach that could be addressed in the future.

One consideration is the trade-off between the tunability gained by the free-space launching used in this work versus an all-fiber integrated configuration by splicing. In previous work we have shown that the ECF can be spliced with standard single mode fibers [25,27,35], and an all-fiber WGM device could be considered in future. Although the spectrum tunability would thus be restricted, a spliced scheme would be practical for real-world sensing applications especially in a reflection configuration with distal end measurements.

Another practical issue is fixing the microsphere resonators onto the ECF. In this work the resonators were held simply by physisorption. To increase the mechanical robustness, other techniques to fix the resonator to the ECF surface could be considered, such as chemical bonding or embedding it into a low refractive index glue as has been reported for lasing or thermal

sensing devices [36,37], noting that the latter would not be suitable for interaction between the micro-coupler and an analyte in liquid or a biological environment.

The efficiency of the coupling to the micro-resonators and the corresponding trade-off with the number of resonators along the fiber should also be considered. That is, subsequent downstream microspheres will have reduced signal intensity due to the induced scattering loss resulting from the upstream microspheres. The evanescent field of the ECF used in this work is relatively small, which is suitable for multi-resonator coupling along a single fiber. On the other hand, a smaller core ECF (e.g., $< 2 \mu\text{m}$ [38]) with a stronger evanescent field could be considered to improve the fiber-resonator coupling efficiency, potentially allowing for use in intensity-dependent lasing or non-linear light generation applications.

The above considerations show the scope of potential advancements beyond our proof-of-concept demonstration, which could be tailored according to the desired application such as nonlinear and quantum optics devices and multi-point sensors and lasers.

Funding. Australian Research Council (ARC) (Future Fellowship (FT200100154)); Optofab node of the Australian National Fabrication Facility utilizing Commonwealth and South Australian State Government Funding; China Scholarship Council (201706750012); ARC Centre for Nanoscale BioPhotonics (CE14010003); National Heart Foundation of Australia (Fellowship 102093); ARC Integrated Devices for End-user Analysis at Low Levels (IDEAL) Research Hub.

Acknowledgments. The authors acknowledge Evan Johnson and Alastair Dowler for their contribution to the fiber fabrication.

Disclosures. The authors declare no conflicts of interest.

Data availability. Data underlying the results presented in this paper are not publicly available at this time but may be obtained from the authors upon reasonable request.

References

1. M. R. Foreman, J. D. Swaim, and F. Vollmer, "Whispering gallery mode sensors," *Adv. Opt. Photonics* **7**(2), 168–240 (2015).
2. L. He, ŞK Özdemir, and L. Yang, "Whispering gallery microcavity lasers," *Laser & Photon. Rev.* **7**(1), 60–82 (2013).
3. F. Vollmer and S. Arnold, "Whispering-gallery-mode biosensing: label-free detection down to single molecules," *Nat. Methods* **5**(7), 591–596 (2008).
4. T. Reynolds, A. François, N. Riesen, M. E. Turvey, S. J. Nicholls, P. Hoffmann, and T. M. J. A. c. Monroe, "Dynamic self-referencing approach to whispering gallery mode biosensing and its application to measurement within undiluted serum," *Anal. Chem.* **88**(7), 4036–4040 (2016).
5. A. François, N. Riesen, H. Ji, S. Afshar V, and T. M. Monroe, "Polymer based whispering gallery mode laser for biosensing applications," *Appl. Phys. Lett.* **106**(3), 031104 (2015).
6. K. Kosma, G. Zito, K. Schuster, and S. Pissadakis, "Whispering gallery mode microsphere resonator integrated inside a microstructured optical fiber," *Opt. Lett.* **38**(8), 1301–1303 (2013).
7. O. Svitelskiy, Y. Li, A. Darafsheh, M. Sumetsky, D. Carnegie, E. Rafailov, and V. N. Astratov, "Fiber coupling to BaTiO₃ glass microspheres in an aqueous environment," *Opt. Lett.* **36**(15), 2862–2864 (2011).
8. A. François, K. J. Rowland, and T. M. Monroe, "Highly efficient excitation and detection of whispering gallery modes in a dye-doped microsphere using a microstructured optical fiber," *Appl. Phys. Lett.* **99**(14), 141111 (2011).
9. J. Lutti, W. Langbein, and P. Borri, "A monolithic optical sensor based on whispering-gallery modes in polystyrene microspheres," *Appl. Phys. Lett.* **93**(15), 151103 (2008).
10. N. M. Hanumegowda, C. J. Stica, B. C. Patel, I. White, and X. Fan, "Refractometric sensors based on microsphere resonators," *Appl. Phys. Lett.* **87**(20), 201107 (2005).
11. J. C. Knight, G. Cheung, F. Jacques, and T. J. O. Birsks, "Phase-matched excitation of whispering-gallery-mode resonances by a fiber taper," *Opt. Lett.* **22**(15), 1129–1131 (1997).
12. F. Lei, R. M. Murphy, J. M. Ward, Y. Yang, and S. N. J. P. R. Chormaic, "Bandpass transmission spectra of a whispering-gallery microcavity coupled to an ultrathin fiber," *Photonics Res.* **5**(4), 362–366 (2017).
13. Y. Ruan, K. Boyd, H. Ji, A. Francois, H. Ebendorff-Heidepriem, J. Munch, and T. M. Monroe, "Tellurite microspheres for nanoparticle sensing and novel light sources," *Opt. Express* **22**(10), 11995–12006 (2014).
14. P. Wang, G. S. Murugan, T. Lee, X. Feng, Y. Semenova, Q. Wu, W. Loh, G. Brambilla, J. S. Wilkinson, and G. Farrell, "Lead silicate glass microsphere resonators with absorption-limited Q," *Appl. Phys. Lett.* **98**(18), 181105 (2011).
15. X. Liu, X. Cui, and D. Wang, "Integrated in-fiber coupler for a whispering-gallery mode microsphere resonator," *Opt. Lett.* **45**(6), 1467–1470 (2020).
16. X. Bai and D. Wang, "Whispering-gallery-mode excitation in a microsphere by use of an etched cavity on a multimode fiber end," *Opt. Lett.* **43**(22), 5512–5515 (2018).
17. R. Wang, M. Fraser, J. Li, X. Qiao, and A. Wang, "Integrated in-fiber coupler for microsphere whispering-gallery modes resonator excitation," *Opt. Lett.* **40**(3), 308–311 (2015).

18. J. Wang, X. Zhang, M. Yan, L. Yang, F. Hou, W. Sun, X. Zhang, L. Yuan, H. Xiao, and T. J. P. R. Wang, "Embedded whispering-gallery mode microsphere resonator in a tapered hollow annular core fiber," *Photonics Res.* **6**(12), 1124–1129 (2018).
19. S. C. Warren-Smith, H. Ebendorff-Heidepriem, T. C. Foo, R. Moore, C. Davis, and T. M. Monro, "Exposed-core microstructured optical fibers for real-time fluorescence sensing," *Opt. Express* **17**(21), 18533–18542 (2009).
20. V. S. Afshar, S. C. Warren-Smith, and T. M. Monro, "Enhancement of fluorescence-based sensing using microstructured optical fibres," *Opt. Express* **15**(26), 17891–17901 (2007).
21. Z. Cai, F. Liu, T. Guo, B.-O. Guan, G.-D. Peng, and J. Albert, "Evanescence coupled optical fiber refractometer based a tilted fiber Bragg grating and a D-shaped fiber," *Opt. Express* **23**(16), 20971–20976 (2015).
22. L. Shi, T. Zhu, D. Huang, C. Liang, M. Liu, and S. J. O. Liang, "In-fiber Mach-Zehnder interferometer and sphere whispering gallery mode resonator coupling structure," *Opt. Lett.* **42**(1), 167–170 (2017).
23. L. Shi, T. Zhu, D. Huang, M. Liu, M. Deng, and W. J. O. Huang, "In-fiber whispering-gallery-mode resonator fabricated by femtosecond laser micromachining," *Opt. Lett.* **40**(16), 3770–3773 (2015).
24. L. Peng, L. V. Nguyen, J. Li, N. Riesen, D. Otten, D. G. Lancaster, H. Ebendorff-Heidepriem, and S. C. Warren-Smith, "Two-dimensional mapping of surface scatterers on an optical fiber core using selective mode launching," *APL Photonics* **6**(2), 026105 (2021).
25. L. Peng, J. Li, R. A. McLaughlin, H. Ebendorff-Heidepriem, and S. C. Warren-Smith, "Distributed optical fiber sensing of micron-scale particles," *Sens. Actuator A Phys.* **303**, 111762 (2020).
26. F. Morichetti, C. Ferrari, A. Canciamilla, A. J. L. Melloni, and P. Reviews, "The first decade of coupled resonator optical waveguides: bringing slow light to applications," *Laser & Photon. Rev.* **6**(1), 74–96 (2012).
27. S. C. Warren-Smith, R. Kosteki, L. V. Nguyen, and T. M. Monro, "Fabrication, splicing, Bragg grating writing, and polyelectrolyte functionalization of exposed-core microstructured optical fibers," *Opt. Express* **22**(24), 29493–29504 (2014).
28. M. F. Limonov, M. V. Rybin, A. N. Poddubny, and Y. S. Kivshar, "Fano resonances in photonics," *Nat. Photonics* **11**(9), 543–554 (2017).
29. Y. Wang, H. Zhao, Y. Li, F. Shu, M. Chi, Y. Xu, and Y. J. P. R. Wu, "Mode splitting revealed by Fano interference," *Photonics Res.* **7**(6), 647–651 (2019).
30. Y. Xiao, V. Gaddam, and L. Yang, "Coupled optical microcavities: an enhanced refractometric sensing configuration," *Opt. Express* **16**(17), 12538–12543 (2008).
31. W. Liang, L. Yang, J. K. Poon, Y. Huang, K. J. Vahala, and A. Yariv, "Transmission characteristics of a Fabry-Perot etalon-microtoroid resonator coupled system," *Opt. Lett.* **31**(4), 510–512 (2006).
32. S. Fan, "Sharp asymmetric line shapes in side-coupled waveguide-cavity systems," *Appl. Phys. Lett.* **80**(6), 908–910 (2002).
33. I. Teraoka and S. Arnold, "Theory of resonance shifts in TE and TM whispering gallery modes by nonradial perturbations for sensing applications," *J. Opt. Soc. Am. B* **23**(7), 1381–1389 (2006).
34. L. Maleki, A. Matsko, A. Savchenkov, and V. Ilchenko, "Tunable delay line with interacting whispering-gallery-mode resonators," *Opt. Lett.* **29**(6), 626–628 (2004).
35. N. P. Mauranyapin, L. S. Madsen, L. Booth, L. Peng, S. C. Warren-Smith, E. P. Schartner, H. Ebendorff-Heidepriem, and W. P. Bowen, "Quantum noise limited nanoparticle detection with exposed-core fiber," *Opt. Express* **27**(13), 18601–18611 (2019).
36. G. Zhao, ŞK Özdemir, T. Wang, L. Xu, E. King, G.-L. Long, and L. J. S. B. Yang, "Raman lasing and Fano lineshapes in a packaged fiber-coupled whispering-gallery-mode microresonator," *Sci. Bull.* **62**(12), 875–878 (2017).
37. F. Monifi, S. K. Özdemir, J. Friedlein, and L. Yang, "Encapsulation of a fiber taper coupled microtoroid resonator in a polymer matrix," *IEEE Photonics Technol. Lett.* **25**(15), 1458–1461 (2013).
38. E. P. Schartner, A. Dowler, and H. J. O. M. E. Ebendorff-Heidepriem, "Fabrication of low-loss, small-core exposed core microstructured optical fibers," *Opt. Mater. Express* **7**(5), 1496–1502 (2017).